Materials and Structures (2025) 58:317
https://doi.org/10.1617/s11527-025-02847-y

ORIGINAL ARTICLE

The role of water during carbonation of highly porous CSA-cement-based thermal insulation plaster

Stefan Zelder · Matheus de Moura Golia · Andreas Rosin · Thorsten Gerdes · Stefan Schafföner

Received: 6 May 2025 / Revised: 17 September 2025 / Accepted: 20 October 2025 / Published online: 30 October 2025

Abstract Reducing the carbon footprint of cement-based materials is a crucial step for a sustainable cement industry. CO_2 emissions from the decalcification of lime during Portland cement production cannot be avoided. Thus, alternative binders such as calcium sulfoaluminate (CSA) cements are becoming more relevant, as they contain a reduced amount of cement clinker and therefore result in lower emissions than Portland cement. In the case of CSA cement, ettringite is primarily formed during hydration, which is susceptible to carbonation over its lifetime. This paper investigates for the first time the carbonation behavior of a porous insulation plaster consisting of micro hollow glass spheres embedded in a needle-like ettringite matrix with an open porosity of approximately 45%. A series of samples were produced in a field trial. On the one hand, the samples were taken from a façade that had been exposed to environmental conditions for two years. On the other hand, comparative samples were stored for two and four years under laboratory conditions. The samples were analyzed for their crystal structure and ratio, thermal conductivity and carbonation rate. Environmental conditions led to 97% carbonation of the ettringite phase after just two years, while a controlled atmosphere led to a carbonation of 76%. It was shown that effective moisture control can significantly slow down the carbonation of highly porous ettringite structures.

Keywords Calcium sulfoaluminate cement · Ettringite · CO_2 uptake · Insulation plaster

S. Zelder (✉) · M. de Moura Golia · A. Rosin · T. Gerdes
Keylab Glass Technology, University of Bayreuth, Prof.-Rüdiger-Bormann-Str. 1, 95447 Bayreuth, Germany
e-mail: stefan.zelder@uni-bayreuth.de

S. Schafföner
Chair of Ceramic Materials Engineering, University of Bayreuth, Prof.-Rüdiger-Bormann-Str. 1, 95447 Bayreuth, Germany

S. Schafföner
Bayerisches Polymerinstitut, University of Bayreuth, Universitätsstraße 30, 95447 Bayreuth, Germany

S. Schafföner
Bayreuther Materialzentrum, University of Bayreuth, Universitätsstraße 30, 95447 Bayreuth, Germany

1 Introduction and background

Insulation materials play an essential role in reducing CO_2 emissions from the building sector [1, 2]. It is estimated that in order to meet the European Union´s emission goals, approximately 1% of the EU´s building stock will need to be renovated each year [3]. Renovation can be carried out, for example, with polymer-based façade insulation materials such as expanded polystyrene, extruded polystyrene or glass wool [4]. As an alternative, a sprayable mineral-based insulating plaster consisting of hollow glass microspheres and a calcium sulfoaluminate (CSA) cement

binder matrix can be used to efficiently insulate old buildings [5].

During the production of CSA cement between 25 and 35% less CO_2/kg are emitted than during the production of ordinary Portland cement [6]. This is due to its decreased lime content, a lower firing temperature during clinker production and lower grinding energy due to its high porosity. In addition to the above steps and efforts to reduce CO_2 emissions from the cement industry, cement has the ability to recapture CO_2 released during the decalcination of lime over its lifetime. All cement-based materials undergo this carbonation process. It is estimated that the total CO_2 emissions from cement production could be considered much lower if, for example, life cycle assessments considered the recapture of CO_2. Between 1930 and 2013, approximately 43% of the CO_2 emissions from cement production (excluding fossil fuel emissions from cement production) were recovered through cement carbonation [7].

The carbonation of cement leads to a phase change in the cement network depending on the type of cement clinker. In CSA cement, ettringite is the dominant hydration reaction product of ye'elimite and anhydrite [8]. Ettringite is a calcium aluminum sulfate phase that is responsible for the fast setting time of CSA cements and their superior mechanical properties after 7 days compared with those of Portland cement [9]. Since ettringite is the dominant phase in hydrated CSA cement microstructure, carbonation leads to a permanent change in phase composition. During the carbonation of ettringite, the following decomposition reaction takes place [10]:

$3CaO \cdot Al_2O_3 \cdot 3CaSO_4 \cdot 32H_2O$	+	CO_2	→	$3CaCO_3$	+	$3(CaSO_4 \cdot 2H_2O)$	+	$Al_2O_3 \cdot xH_2O$	+	$(26-x)H_2O$
ettringite		carbon dioxide		calcium carbonate (calcite)		calcium sulphate (gypsum)		alumina gel		excess water

During carbonation, ettringite is decomposed into three different phases, namely, amorphous alumina hydroxide, crystalline calcium carbonate (calcite) and calcium sulfate (gypsum) [10]. Importantly, even if water does not appear in the equation, the reaction is significantly accelerated in the presence of (adsorbed) water due to the dissolution of calcium ions in water and the formation of $CaOH_2$ [11]. In parallel, CO_2 from the atmosphere dissolves in water and forms carbonic acid. A neutralization reaction then takes place in which calcium carbonate is formed [12]. Calcium carbonate can crystallize in three different polymorphs, namely calcite and the metastable forms vaterite and aragonite [13]. The formation of vaterite and aragonite initially depends on the temperature but will eventually react further to calcite [14]. The rate

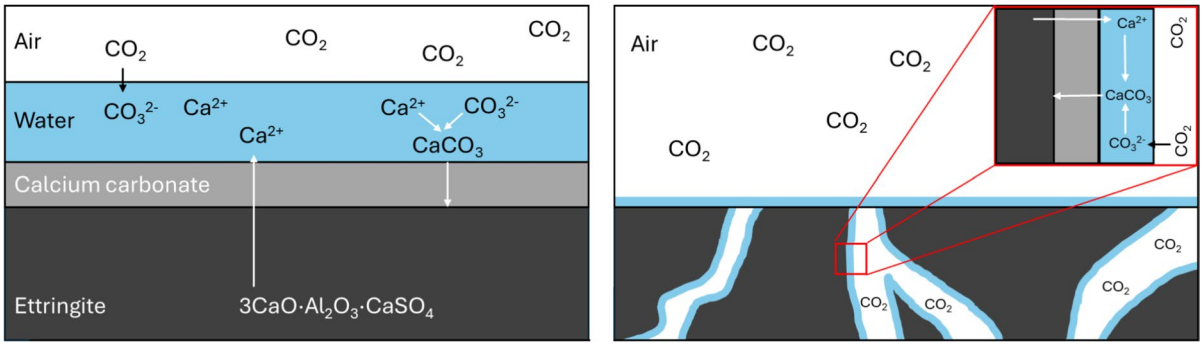

Fig. 1 Schematic illustration of carbonation of ettringite in the presence of water. Left: Carbonation of a dense ettringite phase. Right: Carbonation of a porous ettringite phase

at which ettringite carbonation or calcite formation occurs depends therefore on several factors.

In general, carbonation can be significantly accelerated with increasing humidity [15]. Figure 1 illustrates the process of carbonation of ettringite as either a bulk or porous material. For any dense bulk material (Fig. 1, left side), the carbonation process is a diffusion-controlled process after the formation of an initial calcium carbonate ($CaCO_3$) layer. However, when considering porous ettringite microstructure (Fig. 1, right), carbonation can be significantly accelerated as both reactants—gaseous CO_2 and moisture—can easily access the pore system and initiate the carbonation reaction of ettringite. Pore spaces can increase the reaction area and thus accelerate the carbonation rate.

To date, carbonation rates have been determined either for ettringite powder [16] or for a dense bulk material [17]. By contrast, the present study investigates the real-time carbonation behavior of ettringite needles when utilized in a thermal insulating plaster under field conditions for the first time. The plaster, consisting of hollow glass microspheres and a CSA cement matrix, is highly porous. The hollow glass microspheres employed in the process provide a high surface area for crystallization. Owing to its highly porous, needle-like microstructure, it is to be expected that the carbonation of the ettringite matrix in the described insulating plaster might be accelerated. The possible change in the needle-like Ettringite structure as a result of the carbonation reaction is also of interest, as this contributes significantly to the strength of the plaster. Consequently, a range of samples were analyzed to assess their carbonation behavior. The samples were obtained from a façade that had been exposed to the elements for a period of two years. For the purpose of comparison, insulation plaster samples that had been stored for a period of between two and four years in a laboratory environment under controlled conditions were examined. Due to the differing moisture content and varying storage time, the carbonation rate can be investigated as a function of moisture and time.

2 Materials and methods

2.1 Materials

The plaster used in this study was a mixture of hollow glass microspheres (HGMS) and cement. The HGMS are made of borosilicate glass with a diameter of 20–80 µm, a wall thickness of 1–2 µm and a density of 0.15 g/cm^3 (K15, 3 M, USA). The binder was a CSA cement (Next Base Cement gray, Buzzi Unicem, Italy). Its chemical composition was analyzed by X-ray fluorescence analysis (XRF, ZSX Primus II, Rigaku, Japan) and is provided in Table 1.

Table 1 Oxide composition of CSA cement clinker used in this study determined by X-ray fluorescence analysis

Element	CaO	Al_2O_3	SO_3	SiO_2	Fe_2O_3	TiO_2	MgO	K_2O
Composition [wt.%]	45.7	23.5	19.5	6.3	2.4	1.3	1.0	0.3

Table 2 Overview of the investigated sets of samples of thermal insulation including the way of application, period of use/storage, place of use/storage condition and range of environmental conditions

Sample	Application	Period of use/storage	Place of use/storage	Environmental conditions
28d	Wet spraying	28 days	Humidity chamber	99% rH, 20 °C
2y_fs 2y_fw	Manual plastering	2 years	Exterior façade, shaded location, N48°54′48.554″, E13°21′13.964″	− 18 to 31 °C, 70–86% rH, 80–160 mm/month (precipitation)
2y_is 2y_iw	Manual plastering	2 years	Interior façade (position see above)	66% rH, 19.5 °C, kept constant
4y_s 4y_m	Mold casting	4 years	Indoor	41 ± 3% rH, 20–24 °C

The insulating plaster samples, which were analyzed for carbonation, were prepared and stored under varying conditions. All samples are based on a mixture of 49% CSA cement, 49% HGMS as well as 2% additives to modify the viscosity and setting time. A powder-to-water ratio of 2.2 was used for all the samples. Owing to different methods of application, the manufacturing varied between the collected samples and are specified in Table 2.

The sample "28d" was prepared via wet spraying in a laboratory setup. After spraying, the sample was stored for 28 days in a humidity chamber at 99% rH and 20 °C. The sample was then dried at 40 °C for 24 h.

Furthermore, samples were taken from real insulating layers that were exposed to adverse climatic conditions. Figure 2 provides an overview of the locations of those four sets of samples. The material was applied to the exterior and interior façades of a small test building located in the immediate vicinity of a larger building outside direct sunlight on its north side but not outside the range of driving rain (location: N48°54′48.554″, E13°21′13.964″, Spiegelau, Germany). The façade insulating layer had a thickness of 50 mm. The exterior façade was subject to the seasons and was exposed to temperatures ranging from − 18 to 31 °C and a relative humidity ranging from 70 to 86% [18]. The interior façade insulation layer had a thickness of 40 mm and was exposed to a constant temperature of 19.5 °C and a constant relative humidity of 66%. Both layers were covered with a glass fiber textile, a finishing plaster and a top coat. The samples were taken from the external ("2y_f*x*") and internal façades ("2y_i*x*"), where *x* indicates whether the sample was taken from the surface ("s") or from the side facing the wall ("w").

The sample stored for 4 years were manufactured in a cubic shaped mold ($150 \times 150 \times 150$ mm^3) and deposited under controlled indoor conditions at temperatures ranging from 20–24 °C and an average relative humidity of 41 ± 3%. One specimen was taken from the surface of the cube and labeled "4y_s", another sample was taken from the middle of the cube and labeled "4y_m".

2.2 Methods

2.2.1 X-ray diffraction (XRD)

Phase analysis was performed via X-ray diffractometry (XRD, D8 Discovery A25, Bruker, USA). The device was operated at 40 kV and 40 mA with a copper radiation source (1.5406 Å). A Lynxeye detector was used to record the diffractograms. The measurement range of 2θ was set from 10° to 90°. The samples were rotated at 15 rpm during measurement. The measurement time per step was set to 0.4 s in 0.02° steps. Phase analysis and Rietveld refinement were performed via the open source software Profex (version 5.2.9) [20].

2.2.2 Scanning electron microscopy (SEM)

The microstructure was analyzed by scanning electron microscopy (SEM, FEI Quanta FEG 250, Thermo Fisher Scientific, USA). Before analysis, the samples were dried at 40 °C for 24 h and then coated with a 2 nm platinum layer using a sputter coater (208HR, Cressington, England). The analysis was performed using an acceleration voltage of 5 kV and a secondary electron detector.

2.2.3 Open porosity measurement

The open porosity and density were measured via the Archimedes method. Before measurement, the samples were dried at 40 °C for 24 h. The dry mass was subsequently determined via a scale (ACS 200–4, Kern & Sohn GmbH, Germany). Afterwards, the samples were placed in a desiccator. A lid with holes was placed on top of the samples to prevent them from floating at the surface. The desiccator was closed and evacuated for 30 min. Then, deionized water was added until the samples were completely submerged. Following that step, the desiccator was evacuated for another 30 min. Afterwards, the lid was removed, and the samples were kept under water at atmospheric pressure for another 30 min. After the process, the wet mass and the buoyancy mass were determined. For the determination of the buoyancy mass, the same water used for the infiltration was used. All steps were carried out at 20 °C. The calculation of the open porosity was conducted using Eq. 1.

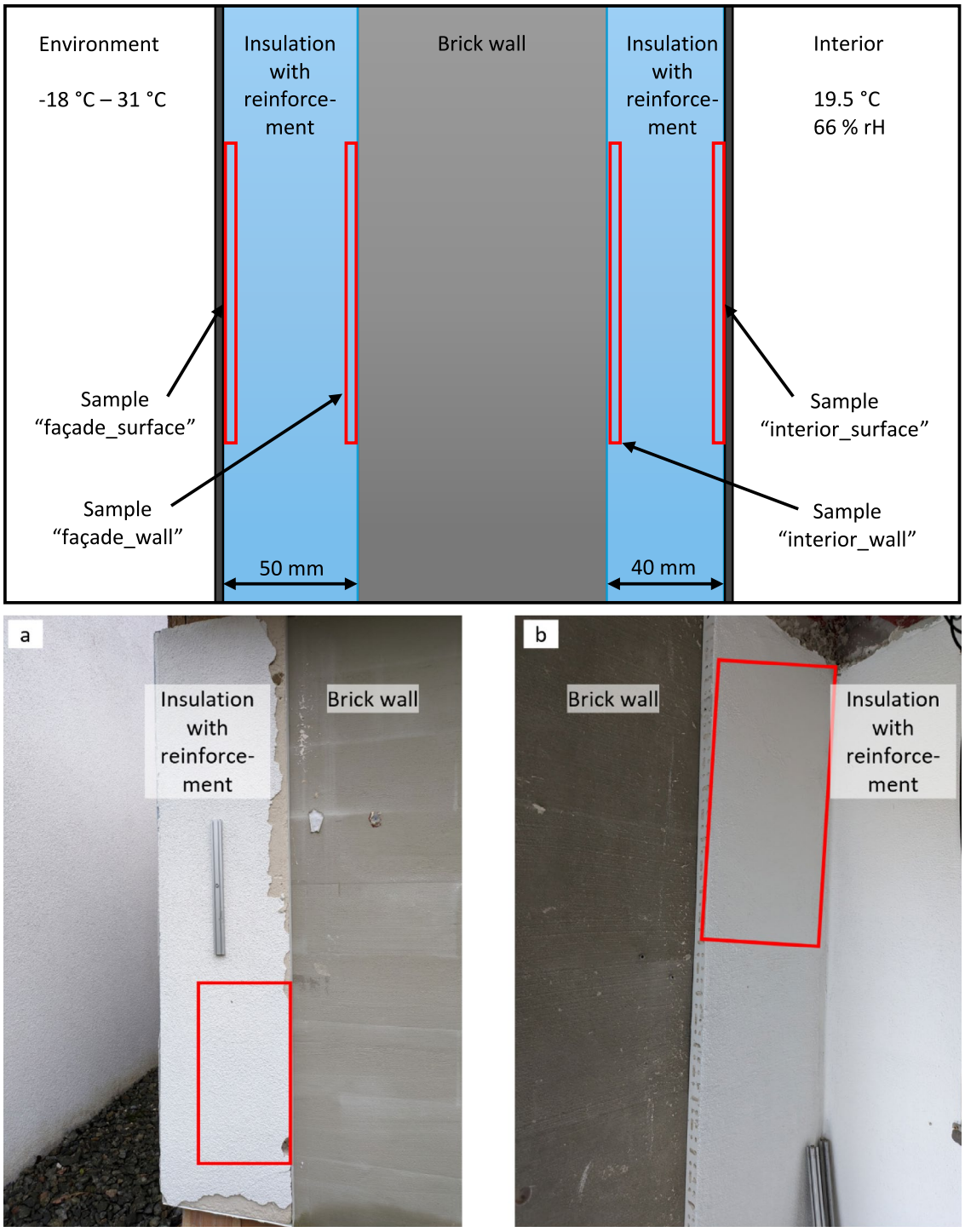

Fig. 2 Top: Cross-section of the façade structure of the test building including the areas where the different samples were taken. Both layers of insulation, internal and external, were covered with a glass fiber fabric as reinforcement, which was removed prior to sampling [19]. Bottom; a: Image of the façade insulation; b: Image of the interior wall insulation

$$\varepsilon = \frac{m_{\text{wet}} - m_{\text{dry}}}{m_{\text{wet}} - m_{\text{buoyancy}}} \quad (1)$$

2.2.4 Thermal conductivity

The thermal conductivity was measured via a surface probe (Isomet 2114, Applied Precision, Slovakia). Each sample was dried at 40 °C for 24 h before measurement. The measurements were conducted in an air-conditioned laboratory at 20 °C. Measurements were performed at three different locations on the same sample.

2.2.5 Mechanical testing

A three-point bending test was performed via a universal testing machine (Inspect duo 10 kN, Hegewald & Peschke, Germany). The load roller spacing was set to 50 mm. The traverse speed was set to 2 mm/min until a preload of 1 N was reached. The speed was then set to 1 mm/min until the sample broke. A 500 N load cell was used.

2.2.6 Thermogravimetric analysis

Thermogravimetric analysis (TG) and mass spectroscopy of the gaseous compounds were performed using a simultaneous thermogravimetry device (STA 449C, Netzsch, Germany). The heating rate was set to 10 K/min up to 1000 °C. The measurements were conducted in air.

2.2.7 Calculation of CO_2 uptake

To determine the theoretical CO_2 binding capacity, the molar mass of ettringite was calculated according to its stoichiometry provided in Eq. 1. Assuming that the binder consists entirely of CSA cement and that the clinker hydrates completely into ettringite within four weeks, the molar mass of the anhydrous ettringite was then determined, which is equated with the molar mass of the CSA cement clinker (Eq. 2).

$$M_{\text{CSA clinker}} = M_{\text{Ettringite}} - 32 \cdot M_{\text{H}_2\text{O}} \quad (2)$$

One mol of ettringite can bind up to three mol of CO_2 because of the presence of the equivalent of three CaO molecules. Taking this into account, the CO_2 binding capacity of ettringite and the CSA cement clinker can be calculated using the mass of one mol ettringite and three mol CO_2 (Eq. 3).

$$m_{\text{CO2maxper kg ettringite}} = \frac{m_{3\text{CO}_2}}{m_{\text{ettringite}}} \cdot 1000 \quad (3)$$

The achieved CO_2 binding capacity of ettringite was calculated according to Eq. 4

$$m_{\text{CO}_2\text{per kg ettringite}} = m_{\text{CO}_2\text{max}} \cdot (100\% - w) \quad (4)$$

where w is the amount of ettringite left in the sample according to Rietveld refinement. These steps were carried out accordingly for the molar mass of the CSA cement clinker.

3 Results

The samples were analyzed regarding their phase composition, microstructure, and thermal behavior. Lastly, the carbonation rate of all samples was calculated. The X-ray diffractograms of the samples stored under controlled indoor conditions are shown in Fig. 3. All samples contained the same crystalline phases, but each had an individual ratio.

The calculated amount of each phase according to Rietveld refinement is provided in Table 3. The most recent sample, which was stored for 28 days ("28d"), contained ettringite as the main hydration phase, calcite and anhydrate. Anhydrate remained from the CSA cement clinker. The samples stored for four years under controlled indoor conditions ("4y_s" or "4y_m") contained much less ettringite than the sample "28d". Instead, the amount of calcium carbonate in the form of calcite, vaterite and aragonite increased. Owing to the advanced carbonation of the sample taken from the surface of the cube, gypsum formed there. However, carbonation was less advanced in the middle of the sample ("4y_m").

Figure 4 shows the diffractograms of the samples taken from the interior ("*i*") and exterior façades ("*f*") of the test building, divided into surface side ("2y_fs" and "2y_is") and wall side ("2y_fw" and "2y_iw").

The phase compositions calculated from Rietveld refinement of the samples taken from internal and

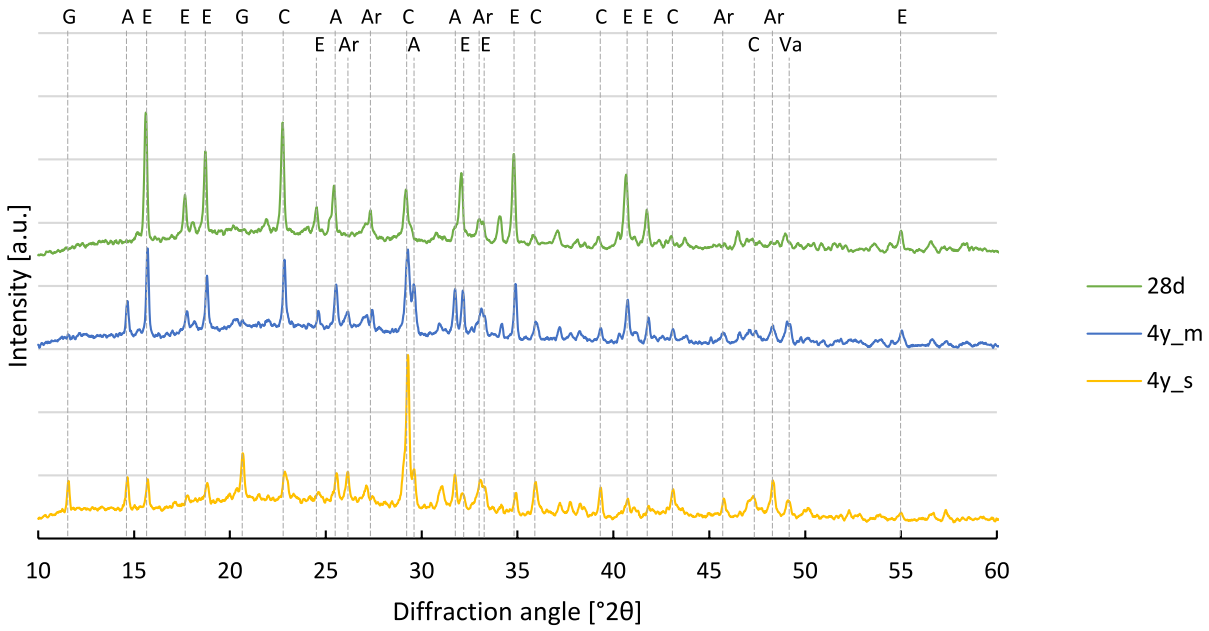

Fig. 3 XRD analysis of the 28 days as well as the 4-year-old sample stored under controlled conditions. (A: anhydrate; Ar: aragonite; C: calcite; E: ettringite; G: gypsum; Va: vaterite)

Table 3 Phase composition according to Rietveld refinement for the 28 days sample as well as the 4-year samples

Phase	28 days	4 years	
	"28d"	"4y_s" (surface)	"4y_m" (middle)
Anhydrate	1.7 ± 0.2	7.3 ± 0.3	7.5 ± 0.3
Aragonite	1.2 ± 0.5	18.6 ± 0.7	12.5 ± 0.5
Calcite	8.5 ± 0.6	28.1 ± 0.6	15.9 ± 0.6
Ettringite	82.7 ± 0.9	24.0 ± 0.8	54.7 ± 0.7
Gypsum	2.3 ± 0.3	17.9 ± 0.8	4.3 ± 0.5
Vaterite	3.6 ± 0.6	4.1 ± 0.6	5.1 ± 0.6

Goodness of fit: 28d: $\chi^2 = 1.37$; 4y_s: $\chi^2 = 1.27$, 4y_m: $\chi^2 = 1.32$

external façade samples are shown in Table 4. After two years of exposure, the amount of the ettringite phase on the internal façade decreased from 82 to 46% on the wall side, and 58% on the surface side. At the same time, the calcite phase increased to 21% and 18%, respectively. On the external façade, the amount of ettringite decreased to 3% on the surface and 19% on the wall-side, whereas the amount of calcite phase increased to 28% and 21%, respectively.

To assess the stability of the gypsum phase, which formed particularly on the "2y_fs" sample, the sample was placed in water at room temperature for 30 days. The crystalline phases were then again investigated by XRD. The corresponding diffractogram is shown in Fig. 5. After storage in water, only calcium carbonate phases remained, namely calcite, vaterite and aragonite.

The microstructure of sample "28d" in Fig. 6 showed hollow glass microspheres and needle-like structures dominated by ettringite crystals. The ettringite crystals were finely dispersed in interstitial spaces, linking the hollow glass microspheres with the binder matrix.

For comparison, Fig. 7 shows SEM images of the aged samples "2y_fs" (a) and "2y_is" (b). Both samples had very similar needle-like structures to sample "28d". The needle-like entities appeared to be in constant contact with the hollow glass spheres and the porous matrix. There was no discernible loss of phase cohesion.

The SEM images did not indicate whether the porosity of the plaster changed during the storage/utilization phase. Therefore, the actual density and the open porosity were determined via the Archimedes method. Table 5 shows the measured mean values for density and open porosity for all the samples. All samples exposed to environmental conditions

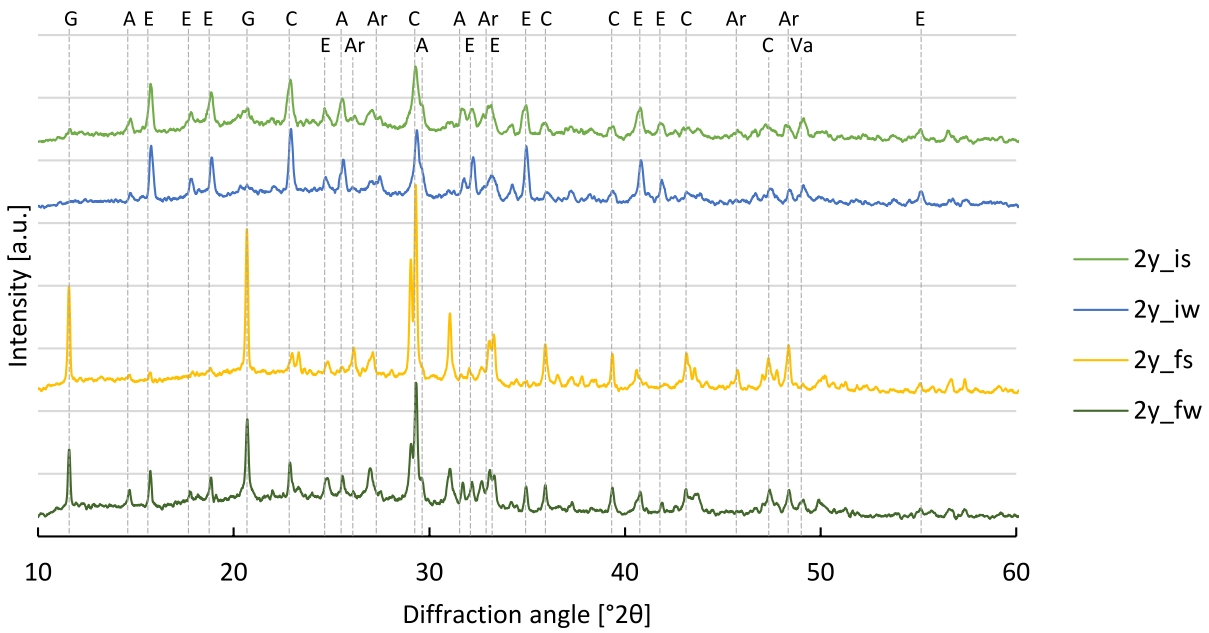

Fig. 4 XRD-analysis of the façade and interior sample. (A: anhydrate; Ar: aragonite; C: calcite; E: ettringite; G: gypsum; Va: vaterite)

Table 4 Phase composition according to Rietveld refinement for the inside applied plaster samples

Phase	2y_interior		2y_façade	
	Surface	Wall	Surface	Wall
Anhydrate	4.1 ± 0.4	2.9 ± 0.3	1.0 ± 0.3	3.5 ± 0.4
Aragonite	9.0 ± 0.6	4.9 ± 0.5	16.8 ± 0.8	2.3 ± 0.5
Calcite	21.5 ± 0.8	18.6 ± 0.7	28.6 ± 0.7	21.8 ± 0.6
Ettringite	46.5 ± 0.9	58.9 ± 0.9	3.2 ± 0.6	19.8 ± 0.7
Gypsum	5.5 ± 0.4	3.0 ± 0.3	36.5 ± 0.8	24.3 ± 0.7
Vaterite	13.4 ± 0.9	11.7 ± 0.8	14.0 ± 0.9	28.3 ± 0.8

Goodness of fit: 2y_is: $\chi^2 = 1.41$; 2y_iw $\chi^2 = 1.31$; 2y_fs: $\chi^2 = 1.48$; 2y_fw $\chi^2 = 1.42$

presented an increase in the open porosity of approximately 20%.

In order to assess the influence of the open porosity regarding the insulation behavior, the thermal conductivity values of the samples were measured. As indicated by the results in Table 6, no significant changes were found with respect to measurement accuracy.

To assess the mechanical stability of the material after carbonation, a three-point bending test was performed to evaluate the flexural strength. Owing to the different manufacturing methods (see Sect. 2), only the two samples "28d" and "4y_m" were compared. As shown in Fig. 8, the flexural strength of the 4-year-old plaster sample decreased to 0.317 MPa compared with that of the sample “28d”, which had a flexural strength of 0.57 MPa.

To confirm the chemical binding of CO_2 during exposure and to assess the possible rate of carbonation, thermogravimetric measurements were carried out to assess any mass changes during heating. A mass loss would most likely occur due to the release of physically and chemically bound water. On the other hand, a loss of mass can also be attributed to the thermal decomposition of carbonates, which is characterized by the release of CO_2 at higher temperatures. For this purpose, samples from the outer façade ("2y_fs") and inner façade ("2y_is") were compared with sample "28d". Figure 9 shows the results of the thermogravimetric analysis of the three samples. With increasing temperature, the mass loss of sample “28d” increased to 21%. The samples from the outer and inner façade surfaces (“2y_fs” and “2y_is”) showed slightly higher mass losses of 28% and 26%, respectively. As sample "28d" did not contain many carbonates (approximately 13%, see Table 3), the increased mass loss of the façade samples indicated

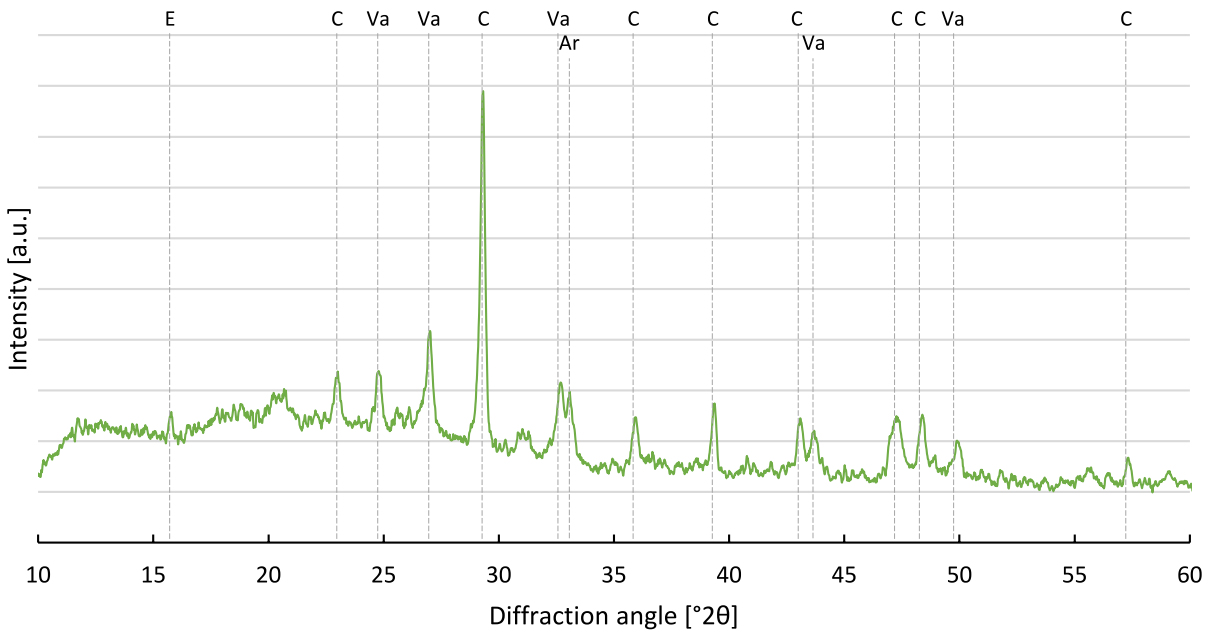

Fig. 5 X-ray diffraction of "2y_fs" after additional exposure for 30 days under water. The measurement time was set to 0.4 s and 0,02° per step and a range from 10 to 70°2Θ. (Ar: aragonite; C: calcite; E: ettringite; Va: vaterite)

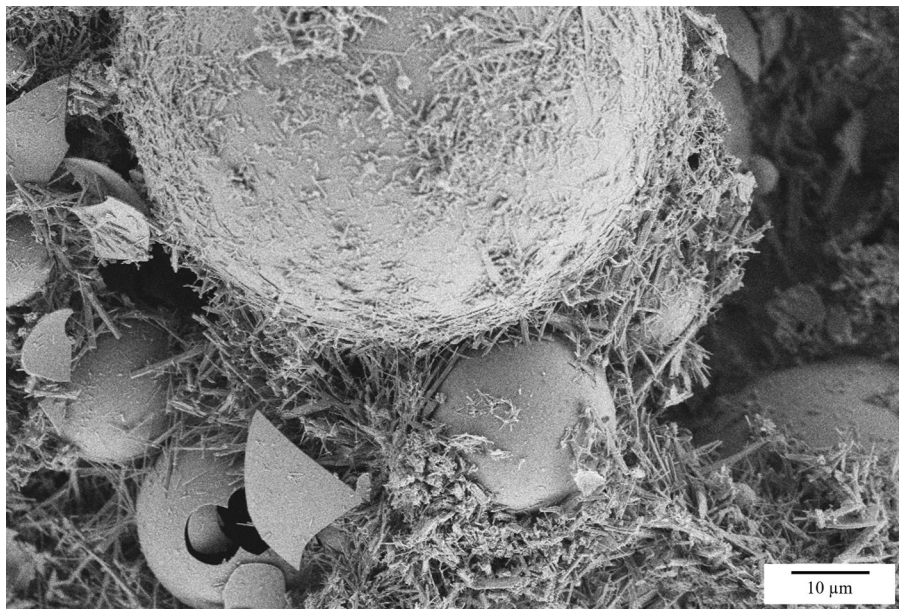

Fig. 6 The SEM image of sample "28d" showed smooth, spherical structures which are hollow glass microspheres as well as glass shards due to broken hollow glass microspheres, and needle-like structures between the spheres which are ettringite crystals

a higher carbonate content in the façade samples, especially for the outer façade. Additionally, the temperature ranges with the greatest mass losses were identified using the first derivative of the TGA data (DTG curves). For all samples, the most significant mass loss was observed around 100 °C and between 650 and 700 °C.

The mass loss rate was not linear over the whole temperature range. In particular, there was a small step in the curve at approximately 730 °C.

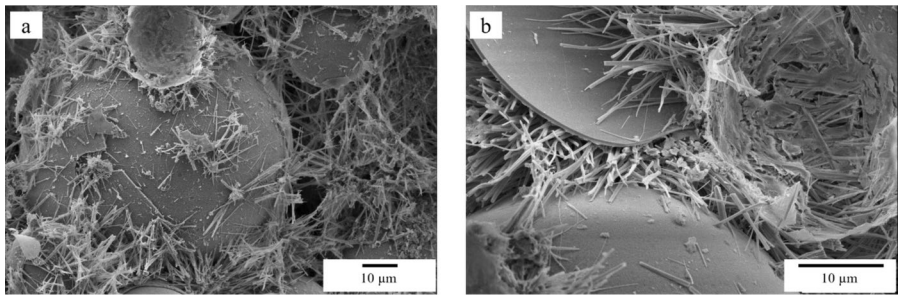

Fig. 7 **a**: SEM image of the sample "2y_fs". **b**: SEM image of the sample "2y_is". The smooth, spherical structures are hollow glass microspheres. There were also glass shards due to broken hollow glass microspheres and needle-like structures between the spheres containing calcium carbonate. Both samples retained a needle like microstructure despite the reduced ettringite content

Table 5 Density and open porosity for all samples

Sample	Density [g/cm^3]	Open porosity [%]
28d	0.20 ± 0.01	49.5 ± 0.1
2y_fs	0.224 ± 0.009	67.3 ± 0.9
2y_fw	0.208 ± 0.002	73.9 ± 1.5
2y_is	0.197 ± 0.002	70.3 ± 0.4
2y_iw	0.199 ± 0.001	71.0 ± 1.0
4y_m	0.175 ± 0.003	74.1 ± 1.7
4y_s	0.179 ± 0.003	77.6 ± 1.5

The measurement was conducted following the Archimedes method (N = 3)

Table 6 Thermal conductivity for all samples

Sample	Thermal conductivity [W/mK]
2y_fs	0.049 ± 0.002
2y_is	0.047 ± 0.003
4y_m	0.046 ± 0.001
28d	0.045 ± 0.001

Each measurement was repeated 5 times on the same spot

According to the gas analysis in Fig. 10, which was carried out simultaneously with the thermogravimetric measurement by mass spectrometry and recording the signal curve for the molar mass M = 44 g/mol, which represents CO_2, two release peaks for CO_2 can be identified for all three samples: (a) a broad band at 400–500 °C and (b) a narrow band at approximately 730 °C, which coincided with the mass loss step observed above.

During its lifetime, ettringite can bind up to 105.2 g CO_2 per kg ettringite. For the CSA cement clinker used in this study, the maximum value was 194.5 g CO_2/kg, which was determined using the maximum CO_2 binding capacity of ettringite. Using the results of the Rietveld refinement, the CO_2 uptake of the samples can be calculated. Table 7 provides the calculated carbonation rates in comparison with the process related CO_2 emission during CSA clinker production, i.e. from the decalcination of limestone and other carbonates. Considering the 28d sample, a carbonation of 10% of the process emissions was calculated. The rate increased to up to 58.3% for the "2y_fs" sample, which showed the highest carbonation rate of all samples.

4 Discussion

As expected, carbonation was observed in all exposed CSA-based insulation samples tested over an extended period of time. All samples tested had an increased open porosity of approximately 70%. However, the rate of carbonation strongly depended on the storage conditions of the samples. X-ray diffraction revealed a general decrease in ettringite, which is the main hydration product of CSA cement [21]. Rietveld refinement was used to calculate the changes in composition. The most recent sample, "28d", had an ettringite content of 82.7%. The plaster showed complete hydration after 28 days, as no ye'elimite remained in the hydrated sample. There was also a

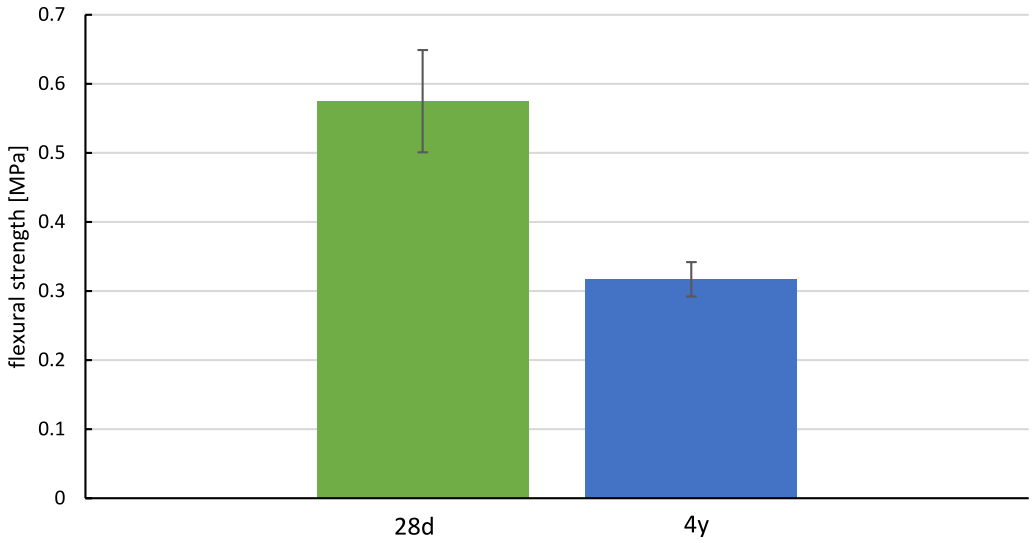

Fig. 8 Flexural strength of the samples "28d" and "4y_m". The measurement was conducted with a 500 N load cell and a measurement speed of 1 mm/min. The samples were taken from the bulk material ("4y_m", N = 3)

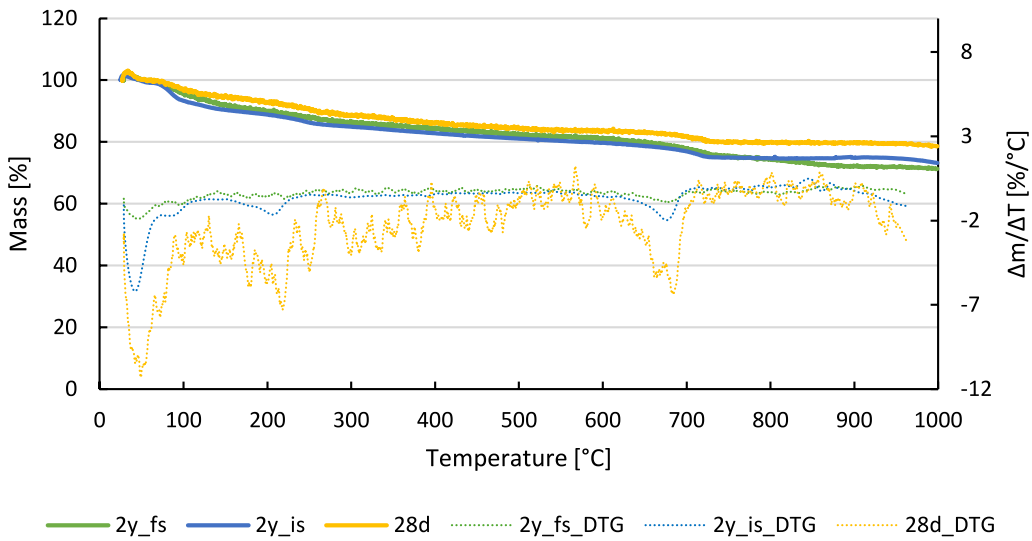

Fig. 9 Thermogravimetric measurement of samples "2y_fs", "2y_is" and "28d" with a heating rate of 10 K/min up to 1000 °C. The measurements were conducted under air. Additionally, the DTG (first derivative of the TGA data) are included to identify temperature ranges with the greatest mass losses. For the derivative, the TGA curves were smoothed using the Savitzky-Golay method (second-order polynomial, window size 200 points)

small amount of anhydrite, which was a remnant of the clinker phase. In addition, 13.3% calcium carbonate was found in the form of calcite, vaterite and aragonite.

For further discussion, we differentiate between the different types of exposure. First, we start with samples "4y_s" and "4y_m", which were stored for four years indoors at a relatively constant humidity of approximately 40% rH and approximately 20 °C. Near the surface ("4y_s"), the proportion of ettringite was reduced to 24%, whereas a fraction of

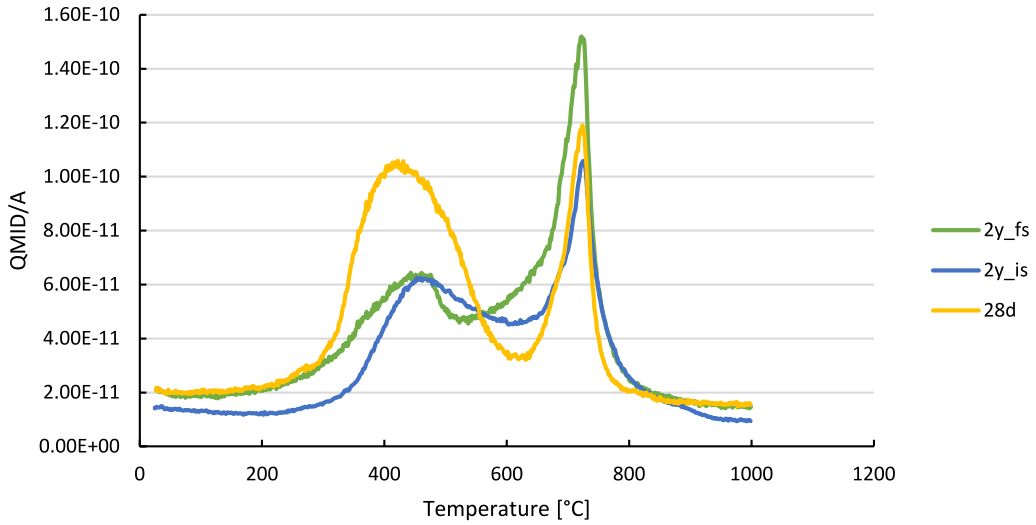

Fig. 10 Release of gaseous CO_2 (M = 44) during thermogravimetric measurement recorded by mass spectroscopy

Table 7 Rate of carbonation for all samples

Sample	Carbonation based on CSA-clinker [g CO_2/kg CSA-clinker]	Retaken process related CO_2 emissions [%]	CO_2 uptake of the process related emissions per year [%/y]
28d	33.7	10.4	–
2y_fs	188.3	58.3	29.15
2y_fw	156.0	48.3	24.15
2y_is	104.2	32.2	16.1
2y_iw	80.0	24.8	12.4
4y_m	88.1	27.3	6.8
4y_s	147.8	45.8	11.4

The amount of g CO_2 /kg CSA-clinker is calculated and compared to the process related CO_2-emissions

approximately 55% ettringite can still be detected far from the surface ("4y_m").

Secondly, the changes in the insulating layer after two years of use on an exterior ("2y_f*x*") and interior façades ("2y_i*x*") are analyzed. The samples aged under adverse climatic conditions such as high humidity, sun, wind, shadows and were frequently exposed to driving rain. For the exterior and interior façades, both near-surface (x = "s") and far-surface (wall-near, x = "w") changes were analyzed. While the proportion of ettringite in the interior façade was reduced to 46% near the surface and 59% far from the surface, the fraction in the exterior façade decreased to 3% near the surface and 20% far from the surface. The fraction of calcium carbonate on the inside increased to 44% near the surface and 35% far from the surface. On the outside, the fraction of calcium carbonate increased to 59% near the surface and 52% far from the surface. In addition, the amount of formed gypsum reached 37% and 26%, respectively. The samples from the outer façade therefore showed a much higher conversion rate of ettringite to carbonates than the samples from the inner façade. Compared with the internal samples ("4y_s/m"), this higher conversion rate was caused by the higher moisture content. In particular, during rain, the external façade can experience exceptionally high levels of moisture ingress. Although a protective plaster with glass fibre reinforcement was applied, it was not sufficiently water repellent to reduce water ingress into the insulation layer. The shaded location of the test building also resulted in longer drying times, which favored accelerated decomposition of ettringite. The rate of conversion of ettringite to calcium carbonate

and gypsum was most likely diffusion controlled [22], as shown by the comparison of samples near and far from the surface. On the other hand, when porous insulating plaster was used indoors, the decomposition of ettringite was less promoted due to reduced access to condensed water phase. The average moisture level was 40% rH at 20 °C for "4y_s" and 66% at 19 °C for "2y_is". This emphasizes the important role that water plays in carbonation. With respect to exposure time the carbonation rate is doubled in sample "2y_is" (66% rH) compared with sample "4y_s" (40% rH). This finding is consistent with previous studies, which described a humidity of 60 to 70% for fast carbonation [15].

Unlike dense cementitious components, the CSA binder used in the insulating plaster exhibits a characteristic crystallization process. Owing to the relatively low volume fraction of approximately 10% by volume and the large pore space, the ettringite phase forms an extensive network of thin, needle-shaped crystals between the micro glass spheres (see Fig. 6). As a result, the processed plaster had an initial open porosity of approximately 45%. After exposure and carbonation, the open porosity increased to about 74% for the sample "4y". The open porosity of the "2y"-samples cannot be compared to the "28d"-samples due to different manufacturing methods, which influence the open porosity. This is attributed to the volume expansion caused by the conversion of ettringite to calcite and gypsum [23]. The carbonation process of these fine ettringite needles follows the same principle as the carbonation of a dense bulk material. However, owing to its high open porosity, gaseous CO_2 and water vapor can easily penetrate the material, undermining the otherwise time-determining diffusion process. It is obvious that the rate of carbonation greatly accelerated by this particular microstructure. The initial carbonate layer also forms on the existing ettringite crystals, but the depth of the material to be penetrated and transformed was considerably less than that in dense cement bodies, as the crystals had diameters of only approximately 1–3 µm. The process is illustrated schematically in Fig. 11.

Another problem associated with the carbonation of insulating plaster is the formation of gypsum during the decomposition of ettringite. When in contact with water, the gypsum phase is soluble [24]. However, this is unlikely to happen to the insulating layer, as it is never exposed to that much condensed water phase, except on the surface during heavy rainfall. This emphasizes the importance of a water-repellent top coat or paint.

Thermogravimetric analysis provides further information for assessing the reabsorbed CO_2 content. The youngest sample ("28d") had a mass loss of approximately 21%, mainly due to the release of chemically bound water from the ettringite crystals [25], with some additional mass loss due to decomposition of carbonates and gypsum at higher temperatures [26]. By contrast, the mass loss of the façade samples increased by approximately 5–7%. This additional mass loss was most likely caused by decarbonation

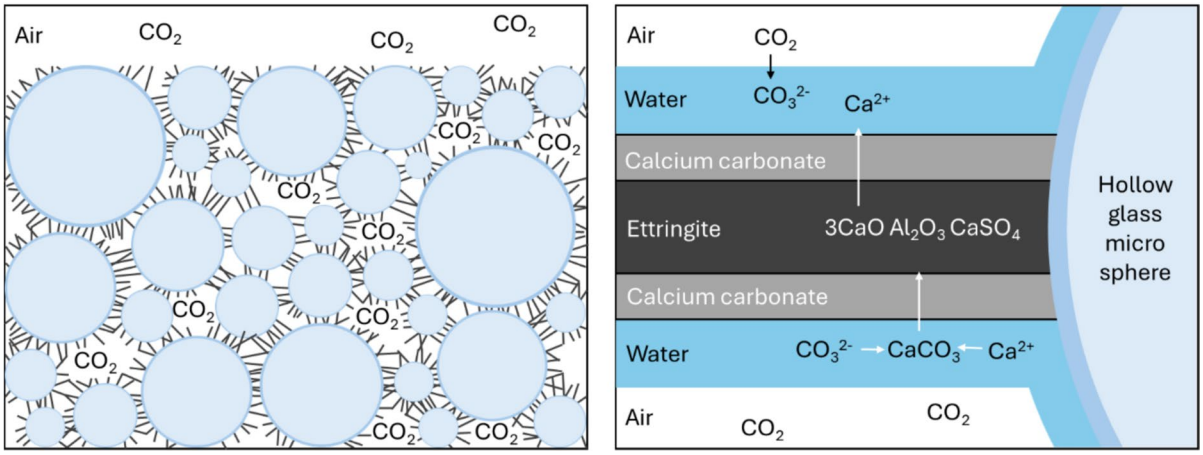

Fig. 11 Schematic illustration of the carbonation process of porous insulating plaster with hollow glass micro spheres (blue spheres) and the fine ettringite crystals (black lines) under moist conditions. (Colour figure online)

of calcium carbonates [27], as simultaneous gas-phase mass spectrometry can detect CO_2 release. The first CO_2 peak at 400–500 °C might be attributed to the combustion of organic components added to increased viscosity and water retention. The second CO_2 peak indicates the decomposition of calcium carbonates. Unfortunately, no quantitative comparison was possible for the analysis of the mass spectrometer data. On the basis of mass loss values and phase analysis by XRD/Rietveld, the façade samples from the test building were clearly exposed to a greater degree of carbonation than the indoor samples were.

Despite the decomposition of ettringite, the microstructure of the matrix was retained, and the needle-like structure was still intact even if little to no ettringite remained. Fernández-Carrasco et al. [28] reported that calcium carbonate can also form needle-like crystals, which was likely the reason for retaining mechanical stability and thermal insulating properties. However, notably, the mechanical strength of the insulating layer also depends on other factors, such as application procedures.

In CSA clinker production a total of 540 g CO_2/kg emissions is generated. Of these, 323 g CO_2/kg are process-related emissions, i.e. from the decalcination of lime stone and other carbonates [29]. Thus, in theory, CSA cement can absorb up to 60% of the process-related emission during carbonation based on the calculated maximum CO_2 uptake of 194.5 g CO_2/kg. The highest amount of carbonation could be achieved with the façade sample with 58.3% of the process-related emissions, which is very close to the theoretical maximum. The samples stored at the façade faced adverse climate conditions. After four years under controlled indoor conditions, 27.3–45.7% of the process related emissions could be absorbed again. These results indicate that carbonation occurs at a highly accelerated rate due to the open porosity of the plaster as well as the fine, needle-like ettringite structure. This assumption is also supported by sample "28d", which exhibited a carbonization of 10.4% after 28 days. This carbonation rate was notably faster in comparison to the carbonation rates observed in the other samples, which were stored for a longer duration. The rapid initial carbonation observed after only 28 days can be attributed to the unique microstructure of the plaster, which enabled the penetration of gaseous CO_2 throughout the entire sample. The finely dispersed ettringite crystals result in a high surface area subjected to carbonation. It is reasonable to expect that the carbonation will slow significantly after the initial carbonate layer forms on the ettringite crystals, as the carbonation process will then be limited by diffusion. Achieving this level of CO_2 binding in just two years is very promising, as it further reduces the carbon footprint of the CSA-cement and can act as a rapid CO_2 sink compared with bulk materials.

Compared to previous studies, the carbonation rate of fine ettringite crystals were determined as a function of moisture content and exposure time. For plaster to be applied on the façade of a building, additional measures must be taken to prevent too much water from being absorbed into the plaster. Further investigations should focus on the influence of hydrophobizing agents on the carbonation rate. This could be an effective measure against too rapid carbonation of the ettringite phase.

5 Conclusion

Sprayable insulation based on HGMS and CSA binder represents a special feature compared to established building insulation systems, whether in terms of the application process and material properties, or due to its ability to absorb a significant proportion of the CO_2 emissions caused by the raw materials used in the production of CSA cement in a relatively short time.

In the present study, fine ettringite crystals were studied for the first time to assess their carbonation rate as a function of moisture and time under realistic climatic conditions in a porous insulting plaster. Samples of the highly porous insulating layers stored for one month to 4 years were analyzed via Rietveld-refined XRD and thermogravimetric data regarding the rate of carbonation depending on their individual environmental conditions. Both humidity and duration of storage significantly influence the rate of carbonation. The samples that were used as the thermal insulation layer for two years on an exterior façade of a test building under mostly moist conditions presented the highest rate of carbonation, 96.8%, on its surface. With increasing distance to the surface, the degree of conversion decreased to 80.2%. In contrast, the insulating layer samples stored indoors for 4 years at approximately 40% rH presented a rate of carbonation of approximately

76% on their surface, and approximately 45.3% inside the material. It is expected that 90% ettringite conversion would be achieved indoors after approximately 10 years. However, the structural and thermal characteristics of the insulating layers are maintained, and a decrease of flexural strength cannot be avoided. Even when considering that the test building was exposed to unfavorable environmental conditions to accelerate the aging of the insulation, the long-term stability of this type of façade insulation likely requires an even more hydrophobic barrier to prevent the penetration of water or moisture into the insulating layer to dampen the carbonation reaction of ettringite. If CO_2 emissions from cement production are eliminated in the future through CCS or CCU processes, this new insulation material would represent a CO_2 sink with an absorption capacity of 22–94 g CO_2 per kg of CSA cement clinker and year.

Acknowledgements The authors would like to thank Lena Geiling (Chair of Electrochemical Process Engineering, University of Bayreuth) for providing the TG and MS measurements as well as Max Schmidt (TAZ Spiegelau) for providing the RFA measurements. The authors would also like to thank the Keylab Electron and Optical Microscopy at the Bavarian Polymer Institute (BPI) for SEM imaging.

Funding Open Access funding enabled and organized by Projekt DEAL.

Data availability Data will be made available on reasonable request.

Declarations

Conflict of interest The authors have no relevant financial or non-financial interests to disclose.

References

1. European Environment Agency. Greenhouse gas emissions from energy use in buildings in Europe [Online], 2021. https://www.eea.europa.eu/en/analysis/indicators/greenhouse-gas-emissions-from-energy (accessed on 28 October 2025)
2. Dombaycı ÖA, Gölcü M, Pancar Y (2006) Optimization of insulation thickness for external walls using different energy-sources. Appl Energy 83:921–928
3. European Commission (2020) In focus: Energy efficiency in buildings. https://ec.europa.eu/info/news/focus-energy-efficiency-buildings-2020-feb-17_en. Accessed 11 Nov 2021
4. Heller N, Flamme S (2020) Waste management of deconstructed external thermal insulation composite systems with expanded polystyrene in the future. Waste Manag Res 38:400–407
5. Zelder S, Rosin A, Helling D, Gerdes T, Scharfe F, Schafföner S (2022) Mineral composite plaster containing hollow glass microspheres and CSA cement for building insulation. Appl Sci 12:1152
6. Hanein T, Galvez-Martos J-L, Bannerman MN (2018) Carbon footprint of calcium sulfoaluminate clinker production. J Clean Prod 172:2278–2287
7. Xi F, Davis SJ, Ciais P, Crawford-Brown D, Guan D, Pade C, Shi T, Syddall M, Lv J, Ji L, Bing L, Wang J, Wei W, Yang K-H, Lagerblad B, Galan I, Andrade C, Zhang Y, Liu Z (2016) Substantial global carbon uptake by cement carbonation. Nat Geosci 9:880–883
8. Winnefeld F, Lothenbach B (2010) Hydration of calcium sulfoaluminate cements: experimental findings and thermodynamic modelling. Cem Concr Res 40:1239–1247
9. Huang G, Pudasainee D, Gupta R, Liu WV (2021) Extending blending proportions of ordinary Portland cement and calcium sulfoaluminate cement blends: its effects on setting, workability, and strength development. Front Struct Civ Eng 15:1249–1260
10. Nishikawa T, Suzuki K, Ito S, Sato K, Takebe T (1992) Decomposition of synthesized ettringite by carbonation. Cem Concr Res 22:6–14
11. Rodriguez-Navarro C, Ilić T, Ruiz-Agudo E, Elert K (2023) Carbonation mechanisms and kinetics of lime-based binders: an overview. Cem Concr Res 173:107301
12. Šavija B, Luković M (2016) Carbonation of cement paste: understanding, challenges, and opportunities. Constr Build Mater 117:285–301
13. Steiner S, Lothenbach B, Proske T, Borgschulte A, Winnefeld F (2020) Effect of relative humidity on the carbonation rate of portlandite, calcium silicate hydrates and ettringite. Cem Concr Res 135:106116
14. Stepkowaka ET, Perez-Rodriguez JL, Sayagues MJ, Martinez-Blanes JM (2003) Calcite, vaterite and aragonite forming on cement hydration from liquid and gaseous phase. J Therm Anal Calorim 73:247–269
15. Chen B, Horgnies M, Huet B, Morin V, Johannes K, Kuznik F (2020) Comparative kinetics study on carbonation of ettringite and meta-ettringite based materials. Cem Concr Res 137:106209

16. Zhou Q, Glasser FP (2000) Kinetics and mechanism of the carbonation of ettringite. Adv Cem Res 12:131–136
17. Zhang L, Glasser FP (2005) Investigation of the microstructure and carbonation of $CS^{-}A$-based concretes removed from service. Cem Concr Res 35:2252–2260
18. Wetterkontor, Wetterrückblick Zwiesel (Bayerischer Wald, 612 m). https://www.wetterkontor.de/de/wetter/deutschland/rueckblick.asp?id=217. Accessed 26 July 2024
19. Steffens O et al. (2023) MAGGIE: Energetische Modernisierung des genossenschaftlichen Wohnquartiers Margaretenau in Regensburg: Musterlösungen für solaroptimiertes Wohnen mit innovativen solaraktiven Baukonstruktionen und einem KI-gestützten Energiemanagement für eine netzdienliche, emissionsarme Strom- und Wärmelogistik Ergebnisbericht, 1st ed., Ostbayerische Technische Hochschule Regensburg, Regensburg
20. Doebelin N, Kleeberg R (2015) Profex: a graphical user interface for the Rietveld refinement program BGMN. J Appl Crystallogr 48:1573–1580
21. Park S, Jeong Y, Moon J, Lee N (2021) Hydration characteristics of calcium sulfoaluminate (CSA) cement/portland cement blended pastes. J Build Eng 34:101880
22. Zajac M, Skibsted J, Durdzinski P, Bullerjahn F, Skocek J, Ben Haha M (2020) Kinetics of enforced carbonation of cement paste. Cem Concr Res 131:106013
23. Santhanam M, Cohen MD, Olek J (2003) Effects of gypsum formation on the performance of cement mortars during external sulfate attack. Cem Concr Res 33:325–332
24. Caselle C, Baud P, Kushnir A, Reuschlé T, Bonetto S (2022) Influence of water on deformation and failure of gypsum rock. J Struct Geol 163:104722
25. Lou Y, Ye Z, Wang S, Liu S, Cheng X (2019) Influence of synthesis methods on ettringite dehydration. J Therm Anal Calorim 135:2031–2038
26. Doleželová M, Scheinherrová L, Krejsová J, Vimmrová A (2018) Effect of high temperatures on gypsum-based composites. Constr Build Mater 168:82–90
27. Villagrán-Zaccardi YA, Egüez-Alava H, de Buysser K, Gruyaert E, de Belie N (2017) Calibrated quantitative thermogravimetric analysis for the determination of portlandite and calcite content in hydrated cementitious systems. Mater Struct 50:1–10
28. Fernández-Carrasco L, Torréns-Martín D, Martínez-Ramírez S (2012) Carbonation of ternary building cementing materials. Cem Concr Compos 34:1180–1186
29. Nie S, Zhou J, Yang F, Lan M, Li J, Zhang Z, Chen Z, Xu M, Li H, Sanjayan JG (2022) Analysis of theoretical carbon dioxide emissions from cement production: methodology and application. J Clean Prod 334:130270